Development of XYZ Flexure Micro-positioning stages based on ETC type two-axis flexure hinges

Junqiang Chen, Zehui Zhong, Huaxian Wei*, Xiaodong Niu

Department of mechanical engineering, College of Engineering, Shantou University, Shantou, China

* corresponding author: hxwei@stu.edu.cn

Abstract:

The development of flexure-based XYZ micro-positioning stages incorporating a novel type of flexure hinges with elliptical transverse cross-sections (ETC) is presented. In comparison to classical two-axis flexure hinges featuring rectangular transverse cross-sections (RTC), parametric studies of both the flexure hinges and the flexure stage were conducted, focusing on stress concentration, motion range, and output decoupling. The results demonstrate that the ETC-based XYZ flexure stage outperforms the RTC-based design in all three aspects. A prototype of the XYZ flexure stage utilizing ETC-type two-axis flexure hinges was developed and experimentally tested, achieving motion errors and parasitic motions of less than 5%. The ETC-type two-axis flexure hinges offer a novel approach for advancing spatial flexure stage design.

Keywords: micro-positioning, flexure stage, XYZ, ETC flexure hinges

1 INTRODUCTION

XYZ micro-positioning stages are of significant importance in various advanced applications, such as elliptical vibration cutting (EVC), laser alignment, nanoindentation, and micro-assembly [1–5]. Flexure mechanisms, also referred to as compliant mechanisms, have emerged as fundamental platforms for developing such stages due to their high precision and rapid response capabilities [6–9]. The motion characteristics of flexure mechanisms heavily rely on the behavior of their flexure hinges, as these hinges are responsible for transmitting and transforming motions within the structure [10–15]. Consequently, the design and performance of flexure hinges critically determine the overall motion characteristics of flexure mechanisms [16, 17].

Various types of flexure hinges have been developed, among which notch-type flexure hinges represent one of the most primitive structures due to their compact design and geometric simplicity [18–22]. As illustrated in Fig. 1, notch-type flexure hinges can be classified based on the number of rotational axes: single-axis, two-axis, and multi-axis configurations [23–28]. For spatial micro-positioning applications, flexure hinges with more than two rotational axes are essential.

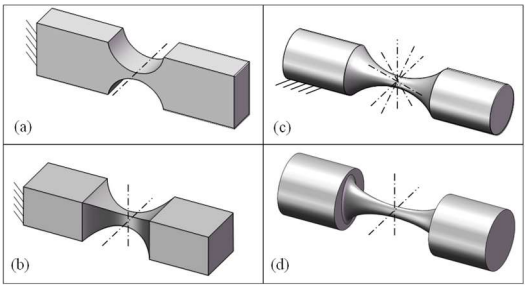

Fig. 1 Primitive notch type flexure hinges: (a) single-axis, (b) RTC type two-axis, (c) multi-axis and (d) ETC type two-axis

While XYZ stages enable translational motions along three orthogonal axes, a key limitation of flexure-based designs is crosstalk between working directions—actuation in one direction may induce parasitic outputs in others [29–31]. To address this issue, researchers have proposed diverse configurations. For instance, Li and Xu

developed a fully decoupled XYZ flexure stage using parallelogram mechanisms [32]. Although this planar structure facilitates fabrication, its large size remains a drawback. Later, Zhu introduced a more compact XYZ flexure stage employing spatial parallelogram mechanisms, which require flexure hinges with out-of-plane deformation capability [33].

In existing studies, two-axis flexure hinges are widely adopted for XYZ flexure stage due to their ease of integration. However, their spatial structures increase fabrication complexity. Recent advancements in 3D printing have enabled practical implementation of such spatial configurations [34, 35]. For instance, Mohammadali developed XYZ stages using two-axis hinges with longitudinally collocated notches [36], while Benjamin created a compact XYZθ stage with built-in actuators via conductive polymer 3D printing [37].

Notably, conventional two-axis flexure hinges typically feature rectangular transverse cross-sections (RTC) with sharp edges that exacerbate stress concentration [38, 39]. A recent innovation introduces elliptical transverse cross-section (ETC) hinges, which eliminate sharp edges while maintaining two-axis motion capabilities [40]. Existing study shows that ETC hinges exhibit enhanced compliance and reduced stress concentration under equivalent displacement actuation. Nevertheless, the performance of ETC-based flexure mechanisms remains understudied.

All three classical primitive hinge types can share identical longitudinal cross-sectional notch profiles at intersections with planes through their central axes. These profiles-constructed using cycloidal, elliptical, hyperbolic, or hybrid curves-significantly influence hinge characteristics. For example, leaf-type hinges demonstrate higher compliance, while cycloidal profiles improve rotational accuracy and reduce stress. However, while notch profiles determine transverse cross-sectional variations, they cannot fundamentally alter cross-sectional types. The four hinge groups are ultimately distinguished by their transverse cross-sections.

This study investigates an XYZ micro-positioning stage utilizing ETC two-axis flexure hinges, achieving systematic analyses and comparisons with classical designs based on RTC flexure hinges. The subsequent sections are organized as follows. The structural design of both the ETC flexure hinges and the XYZ stage is first presented in Section 2, which clarifies the relationships and differences between the two classes of flexure structures. Based on the established parametric model, a comparison of both the flexure hinges and the flexure stages is conducted through parametric analyses in Section 3. Prototyping and experimental studies are detailed in the next section, and conclusions are drawn finally.

2 STRUCTURAL DESIGN

2.1 Configuration of the XYZ Flexure Stage

The configuration of the XYZ flexure stage is first developed, following the design philosophy of flexure substitution. The stage employs a three-limb parallel configuration, where each limb is independently driven by an actuator for unidirectional translation, as shown in Fig. 2. The translational input is directly transformed to the output platform, providing target output motion in identical directions. A decoupling mechanism is employed between each input and the output platform, isolating the unidirectional target output from other inputs. Therefore, the driving direction of each actuator is orthogonal to the working plane of the decoupling mechanism. Piezoelectric stack actuators (PSAs) and voice-coil motors are two of the most common drivers for flexure-based micro-

positioners. In this study, the PSA is employed to achieve a compact design.

To minimize potential parasitic motions, the output axes of the three actuation units are designed to intersect at one point on the output platform. As a result, undesired internal moments are reduced synchronously. The configuration of the stage, as shown in Fig. 2, includes identical actuation units for the X, Y, and Z axes. Since flexure mechanisms are employed to construct the XYZ stage, it is reasonable to customize the stiffness and motion range of each actuation unit through the parametric design of the flexure hinges. The parametric model of the flexure stage is obtained through structural design.

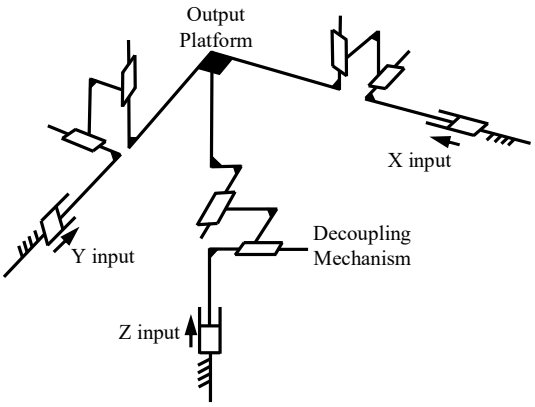

Fig. 2 Configuration of the XYZ flexure stage

2.2 Structural design of flexure hinge

The structural design of flexure hinges primarily focuses on the design of ETC-type two-axis flexure hinges. Two structural design methods are developed for the ETC-type flexure hinges: the replacement method and the direct modeling method. Traditionally, two-axis flexure hinges are constructed by forming orthogonally collocated notches on a rigid bar. This approach essentially creates flexure structures with variable rectangular transverse cross-sections. Consequently, ETC-type two-axis flexure hinges can be derived by replacing the rectangular cross-sections of RTC hinges with elliptical counterparts. As a result, the longitudinal notch profiles of the obtained ETC-type flexure hinges remain identical to those of the RTC designs. This enables seamless conversion between conventional two-axis hinges and the novel ETC variants.

An alternative fabrication method for the ETC flexure hinges, namely the direct modeling method, involves creating an ellipse on the o-yz plane with its origin aligned to the y and z axes, followed by forming notch profiles on the o-xy and o-xz planes. The ETC hinges are then generated by scanning the ellipse while maintaining a fixed orientation and controlled semi-axis variations. Both design methods can obtain identical parametric models of the ETC-type two-axis flexure hinges, as shown in Fig. 3.

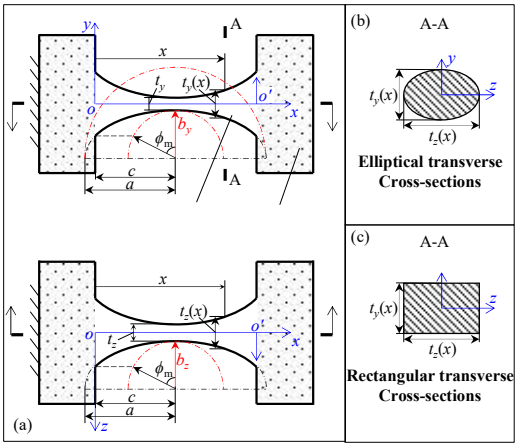

Fig. 3 Notch profiles and transverse cross-sections of ETC and RTC flexure hinges.

The ETC hinges in this study employ right circular-type notch profiles, considering their concise geometry (Fig. 3a and Fig. 3b), characterized by the circular notch radius (R) and minimum thicknesses on the o-xy (t_y) and o-xz (t_z) planes. One of the key observations of the ETC structure is the achievement of axial symmetry (multi-axis flexure hinge) by requiring $t_y = t_z$. In addition, the RTC hinges and ETC hinges can be represented using identical geometrical parameters due to the structural similarity, which is referred to as the equivalent configuration in this study.

2.3 Structural design of the XYZ flexure stage

Flexure mechanisms can be designed by replacing rigid pivots in the configuration with flexure hinges. Flexure replacements are carried out using a modular approach. The decoupling mechanism between the output platform and each input requires compound decoupling capability to achieve spatial motions. Therefore, a spatial four-bar-type parallel decoupling mechanism (PDM) is employed, typically utilizing ETC-type two-axis flexure hinges. In addition, a planar guiding mechanism is utilized to protect the fragile PSA, where leaf-type single-axis flexure hinges are employed. Subsequently, three actuation units are developed, each including a PDM and a guiding mechanism embedded with a PSA. The planar double parallelogram mechanism, incorporating four leaf-type single-axis flexure hinges. The PDM consists of four sets of parallelogram limbs, each constructed from a rigid link and two ETC flexure hinges.

The XYZ flexure stage is obtained by connecting the three actuation units in a parallel configuration, as shown in Fig. 4. Each actuation unit consists of identical flexure modules but can be customized through hinge design. Typically, asymmetric compliances of the stage along the z-axis are designed for potential applications in nanoindentation, which is achieved by controlling $t_y = t_z = t$ for the two-axis flexure hinges within the z-actuation unit. The three actuation units share identical values for the remaining parameters, which mainly include the minimum thickness of the leaf hinge t_h, the radius of the fillet r, and the lengths of the rigid links L, L_1, L_2, and L_3.

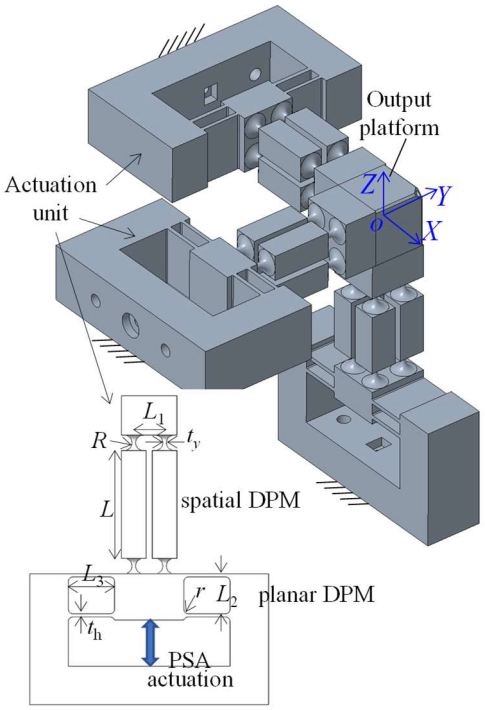

Fig. 4 XYZ flexure stage based on the ETC-type flexure hinges

3 PARAMETRIC ANALYSES

To understand the relationship between the hinge type and the performance of the flexure stage, systematic parametric analyses are carried out. In these analyses, key parameters of the two-axis flexure hinges are varied to observe their effects on the stress and motion characteristics of the flexure stage. Such comparisons are helpful for predicting behavior and guiding decisions in future design and optimization efforts.

3.1 Analyses of the ETC and RTC flexure hinges

The first parametric analyses compare the stress characteristics of ETC and RTC hinges with reference to the stress concentration factor (SCF), defined as the ratio of FEA-derived maximum stress to analytical maximum stress. The stress concentration characteristics of notch-type flexure hinges are primarily influenced by the loading type and the radius of curvature of the notch profile. Without loss of generality, the stress concentration characteristics of the flexure hinges

under tension and pure moments around the y-axis and z-axis are examined.

Under tensile force, the analytical maximum stress is uniformly distributed across the minimum cross-section, which can be obtained as

$$\sigma_{\mathrm{F}x}^{\max} = \frac{4F_x}{\pi t_y t_z} \tag{1}$$

and

$$\sigma_{\mathrm{F}x}^{\max} = \frac{F_x}{t_y t_z} \tag{2}$$

for the ETC and RTC type flexure hinges, respectively.

The analytical normal stresses generated by moments around y-axis or z-axis vary linearly over the transverse cross-section, where the maximum occurs on the outer surface of the cross-section, which can be given as

$$\begin{cases} \sigma_{\mathrm{M}y}^{\max} = \frac{32M_y}{\pi t_y t_z^2} \\ \sigma_{\mathrm{M}z}^{\max} = \frac{32M_z}{\pi t_y^2 t_z} \end{cases} \tag{3}$$

and

$$\begin{cases} \sigma_{\mathrm{M}y}^{\max} = \frac{6M_y}{t_y t_z^2} \\ \sigma_{\mathrm{M}z}^{\max} = \frac{6M_z}{t_y^2 t_z} \end{cases} \tag{4}$$

for the ETC and RTC type flexure hinges, respectively.

The SCF can be obtained as:

$$k = \frac{\sigma_{\mathrm{r}}}{\sigma_{\mathrm{n}}} \tag{5}$$

where σ_{n} is the reference maximum stress calculated using analytical equations (Eq. 1~4.) and σ_{r} is the actual maximum stress within the hinge obtained through FEA.

FEA models were established for the ETC and RTC flexure hinges. The FEA setup utilizes aluminum alloy material properties (E=71 GPa, μ=0.33) with cantilever boundary conditions and mesh refinement in the notch regions. Mesh models with approximately 100,000 nodes and 67,000 elements were achieved, with verification of grid independence. Parametric models of the ETC flexure hinges and their equivalent RTC flexure hinges were developed based on Fig. 3. The curvature of the notch was controlled by varying the radius $R = 2\sim6$ mm and $t_y = 1\sim3$mm, while t_z was fixed at 1 mm. The length of the rigid blocks connected to the two ends of the flexure hinge was also controlled to be twice the length of the hinge to ensure consistent loading conditions. During the analyses, identical cantilever-type boundary conditions were applied to each hinge sample, with one end fixed and the other end loaded with a single type of unit load (F_x, M_y, or M_z) separately.

The SCF under tension and moments were obtained for the ETC and RTC flexure hinges, as shown in Fig. 5 to Fig. 7. It can be observed that the stress concentration is consistently lower for the ETC flexure hinges compared to their equivalent RTC flexure hinges. This is because the stress distributions within the ETC flexure hinges are more uniform than those within the RTC flexure hinges, as the elliptical transverse cross-sections eliminate sharp vertices. For both types of flexure hinges, the SCF is influenced by their geometric parameters. The SCF increases as the notch radius decreases or the minimum thickness increases. Notably, the ETC flexure hinges can achieve stress release when the hinge thickness along the bending direction is lower than that along the other direction, as shown in Fig. 7, suggesting a novel approach for designing flexure mechanisms with a higher compliance-to-stress ratio. It can be concluded that the ETC flexure hinges effectively reduce the effects of stress concentration compared to the RTC flexure hinges.

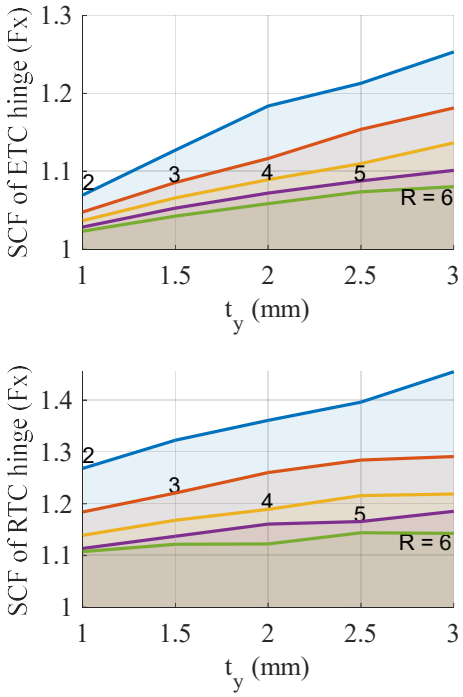

Fig. 5 Stress concentration factor (SCF) of the ETC and RTC flexure hinges under unit tension loading

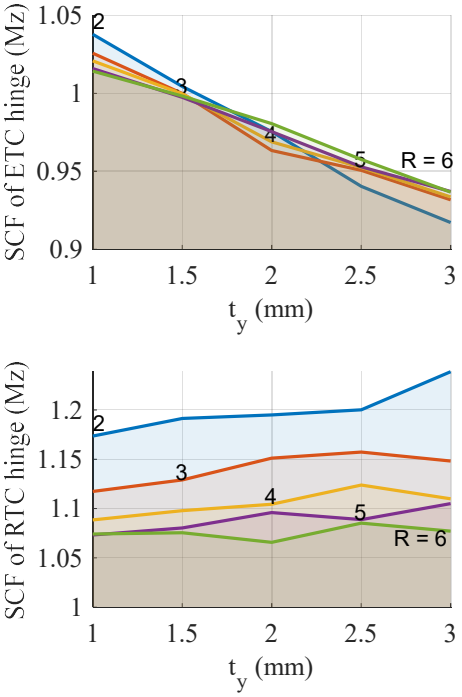

Fig. 7 Stress concentration factor (SCF) of the ETC and RTC flexure hinges under unit moment Mz loading

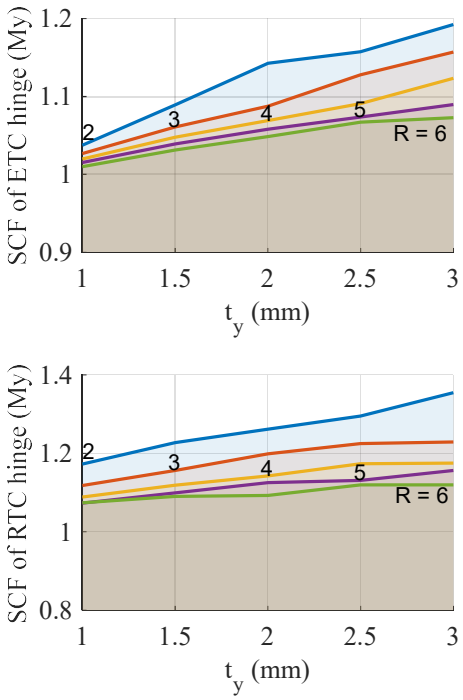

Fig. 6 Stress concentration factor (SCF) of the ETC and RTC flexure hinges under unit moment My loading

3.2 Analyses of the ETC-based and RTC-based XYZ flexure stage

Similarly, two types of XYZ stages embedding ETC and RTC flexure hinges were developed and compared. Due to the monolithic structure of the flexure stage, driving motions from a single PSA induce parasitic motions in other directions, increasing the difficulty of precision control. Meanwhile, the stress level of the structure constrains the motion range of the entire stage. Therefore, both the stress and motion performances of the stage were investigated with reference to the geometric design of the flexure hinges.

Parametric models of both types of flexure stages were developed based on Fig. 4, with a focus on the influence of the two-axis flexure hinges. Considering the asymmetry of the two-axis flexure hinge, only one of the minimum hinge thicknesses was varied ($t_y = 1\sim3$), while the

other was kept at $t_z = 0.75 \times t_y$. The radius of the hinge notch was fixed at $R = 5$ mm to account for manufacturing constraints. Additionally, the minimum thickness of the hinge on the Z-actuation unit varied synchronously by setting $t = t_y$ mm. This approach covers designs with both high and low asymmetric compliance. Key parameters of the flexure stage include the minimum thickness of the leaf hinge ($t_\mathrm{h} = 2$ mm), the radius of the fillet ($r = 3$ mm), and the lengths of the rigid links ($L = 70$ mm, $L_1 = 20$ mm, $L_2 = 26$ mm, and $L_3 = 30$ mm).

FEA based on high-resolution models of the flexure stage was utilized to obtain accurate information on both stresses and motions. Similar FEA settings to those used in the analyses of flexure hinges were applied to the stage. Mesh models with over 3,000,000 nodes and 1,000,000 elements were achieved during the analyses. A typical mesh model of the ETC-based flexure stage is shown in Fig. 8(a).

During the analyses, each actuation unit was successively motivated by a unit force to simulate the actuation of the PSA. The three-coordinate displacement vector at the center of the output platform was recorded, from which the main output and parasitic motions were derived. For instance, when the x-direction was actuated, the displacements along the y- and z-directions were monitored as parasitic motions, while the displacement along the x-axis was defined as the main output. For comparison, the stress levels of the two-axis flexure hinges were measured during the analyses.

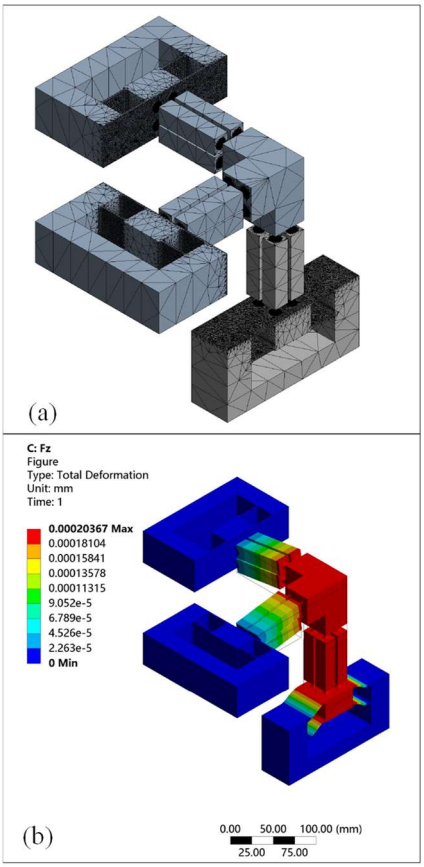

Fig. 8 Mesh model (a) and deformation (b) of the ETC flexure stage under Z actuation

As shown in Fig. 9, the maximum stress levels are consistently lower on the ETC-based stage compared to those on the equivalent RTC-based stage, which aligns with the results of the hinge analyses. In addition, the output motions of the ETC-based stage are greater under identical driving forces, as shown in Fig. 10 to Fig. 12. This suggests that the ETC-based flexure stage achieves higher motion transformation efficiency. Moreover, compared to the equivalent RTC-based flexure stage, the ETC-based stage also exhibits lower parasitic motions, even with larger output motions. Parasitic motions of less than 1%, relative to the main outputs, are observed for all design samples of the ETC-based flexure stage, indicating excellent decoupling performance. It can be concluded that the XYZ flexure stage developed using ETC-type two-axis flexure hinges, compared to the classical RTC-type two-axis flexure hinges, achieves superior

performance in stress levels, motion range, and decoupling characteristics.

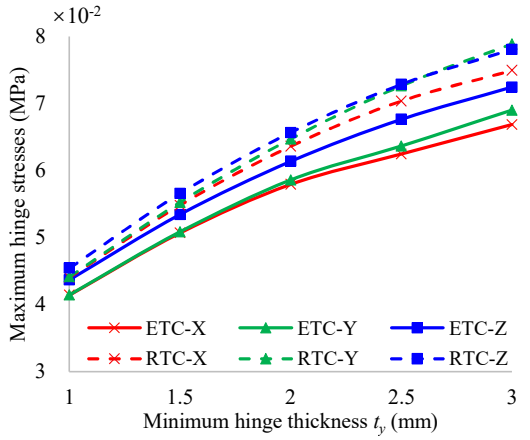

Fig. 9 Maximum hinge stresses of the XYZ stage based on the ETC and RTC flexure hinges under unit actuating forces

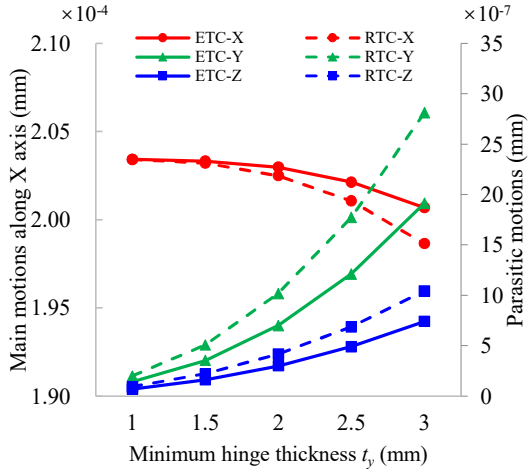

Fig. 10 Main motions and parasitic motions of the XYZ stage based on the ETC and RTC flexure hinges under unit actuating forces along X axis

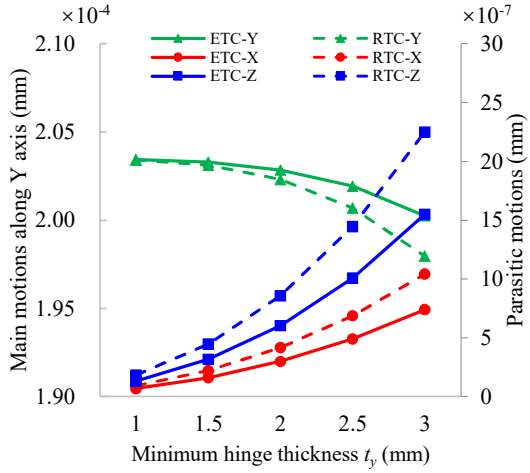

Fig. 11 Main motions and parasitic motions of the XYZ stage based on the ETC and RTC flexure hinges under unit actuating forces along Y axis

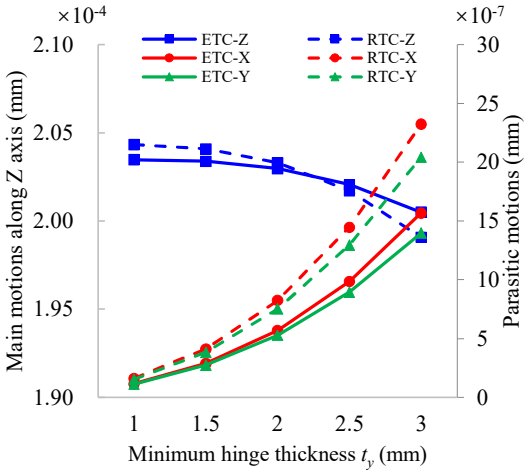

Fig. 12 Main motions and parasitic motions of the XYZ stage based on the ETC and RTC flexure hinges under unit actuating forces along Z axis

4 PROTOTYPE AND EXPERIMENTAL TESTS

A prototype of the XYZ flexure stage based on the ETC-type two-axis flexure hinges was developed and experimentally tested. The structural parameters of the stage were designed to meet the requirements of additive manufacturing, as specified in Table 1. The prototype was fabricated using 3D printing with resin material (R4600, WeNext). A test bench was set up, as shown in Fig. 13, with a PSA actuator (AE0505D16F, Thorlabs) embedded within each actuation unit. Three laser sensors (Keyence, LK-G30) were used to measure the displacements of the output platform.

Table. 1 Key parameters of the fabricated XYZ flexure stage (mm)

t_y	t_z	t	t_h	R	r	L	L_1	L_2	L_3
2	3	2	2	5	0.5	30	15	8	20

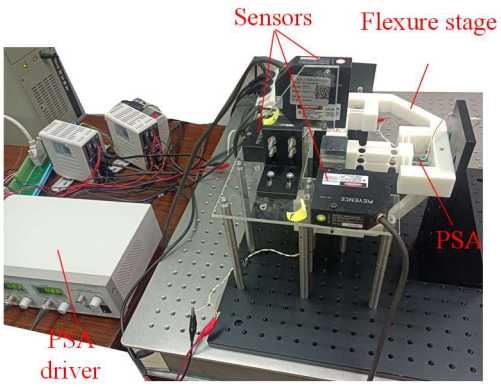

Fig. 13 Prototype of the XYZ flexure stage and apparatus for experiment

Experimental investigations were conducted to assess the motion characteristics of the flexure stage. The outputs of the flexure stage were first investigated through an open-loop test, where each PSA was driven by a ramp signal. It was found that the flexure stage achieved an open-loop motion range of over 10 μm along each motion direction, as shown in Fig. 14. Additionally, parasitic motions were observed during the tests. However, the parasitic outputs were linearly related to the inputs, which can be attributed to manufacturing and assembly errors.

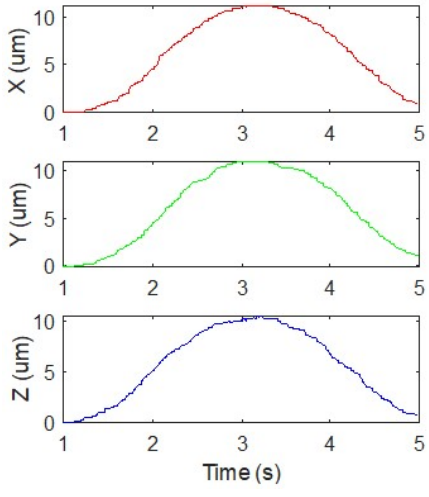

Fig. 14 Output motions of the XYZ flexure stage

Based on the coupling outputs collected during the open-loop tests, a kinematic-based decoupling control strategy was developed for the fabricated XYZ flexure stage. To account for the hysteresis of the PSA, a fundamental PID control method was utilized. Since the motion range is limited, the static outputs of the laser-based displacement sensors were first measured. It has been observed that the static output signal of the sensor is subject to considerable noise interference. Subsequently, mean filtering was applied to reduce the sensor noise. The output platform was successively driven to follow a sinusoidal signal in each direction. As shown in Fig. 15 and Fig. 16, each direction of the developed flexure stage achieved motion tracking with motion errors and parasitic motions of less than 5%.

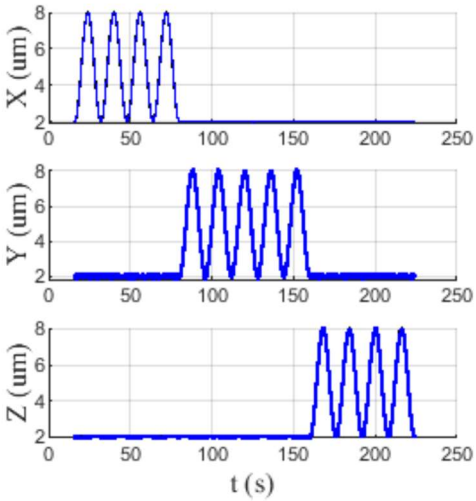

Fig. 15 Decoupled outputs of the XYZ flexure stage

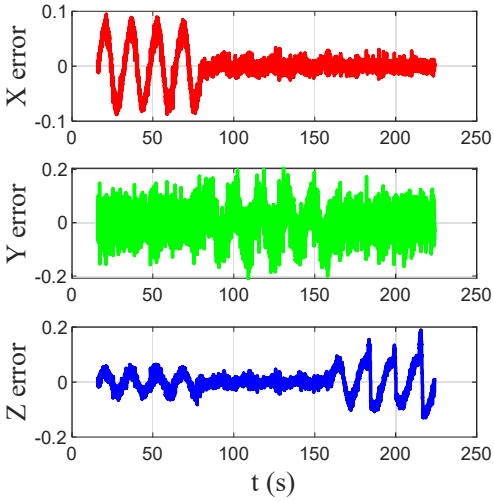

Fig. 16 Motion error and parasitic motions of the XYZ flexure stage

The control accuracy could be further improved by using sensors with higher resolution and lower

noise. Since stress within a real flexure structure is difficult to measure, alternative approaches such as fatigue testing could be employed and will be explored in future work. Another limitation of the flexure stage developed using ETC-type flexure hinges is its fabrication adaptability, as additive manufacturing is generally required to integrate them into spatial structures. Structural stiffness, creep deformation, and fatigue life should also be considered as critical design aspects. Metallic additive manufacturing may be necessary for long-life applications. Nevertheless, the analytical and experimental results validate the feasibility of developing XYZ flexure stages based on ETC-type two-axis flexure hinges for micro-positioning applications.

5 Conclusions

In this research, an XYZ flexure stage was developed utilizing ETC-type two-axis flexure hinges for micro-positioning applications. Systematic comparisons were conducted at both the flexure hinge and flexure stage levels, revealing the relationships between key geometric parameters of the ETC flexure hinges and structural performance. The XYZ flexure stage based on ETC-type two-axis flexure hinges demonstrated superior performance in stress levels, motion range, and decoupling characteristics compared to the flexure stage based on classical RTC-type two-axis flexure hinges. A prototype of the XYZ flexure stage incorporating ETC-type two-axis flexure hinges was developed and experimentally tested, achieving motion errors and parasitic motions of less than 5%. These results validate the feasibility of developing XYZ flexure stages using ETC-type two-axis flexure hinges for micro-positioning applications.

Acknowledgment

We gratefully acknowledge the support received for this work from various funding sources. Specifically, This work was supported by the National Natural Science Foundation of China No. 52305027; the Science and Technology Planning Project of Shantou No.STKJ2024080; and the University-Industry Collaborative Education Program No.241006517305935.

Declarations Competing interests

The authors declare that they have no competing interests that could have appeared to influence the work reported in this paper.

References

1. Han J, Lin J, Li Z, Lu M, Zhang J (2019) Design and Computational Optimization of Elliptical Vibration-Assisted Cutting System With a Novel Flexure Structure. IEEE Transactions on Industrial Electronics 66:1151–1161
2. Zhang X, Cui Y, Yang Y, Lu J, Sun J (2023) Design, analysis, and experiment of a piezoelectric stick–slip rotary actuator with asynchronous-driven dual stators. Mechanical Systems and Signal Processing 200:110524
3. Liu P-B, Yan P, Zhang Z, Leng T-T (2015) Flexure-hinges guided nano-stage for precision manipulations: Design, modeling and control. International Journal of Precision Engineering and Manufacturing 16:2245–2254
4. Ling M, Howell LL, Cao J, Chen G (2020) Kinetostatic and dynamic modeling of flexure-based compliant mechanisms: A survey. Applied Mechanics Reviews. https://doi.org/10.1115/1.4045679
5. Tang C, Zhang M, Cao G (2017) Design and testing of a novel flexure-based 3-degree-of-freedom elliptical micro/nano-positioning motion stage. Advances in Mechanical Engineering 9:168781401772524
6. Shi H, Duan X, Su H-J (2014) Optimization of the workspace of a MEMS hexapod nanopositioner using an adaptive genetic algorithm. IEEE, pp 4043–4048
7. Jin M, Zhu B, Mo J, Yang Z, Zhang X, Howell LL (2020) A CPRBM-based method for large-deflection analysis of contact-aided compliant mechanisms considering beam-to-beam contacts. Mechanism and Machine Theory 145:103700
8. Jin Y, Su H-J (2024) A Compliant Hinge Joint Driven by the PneuNets Bending Actuator. Journal of Mechanisms and Robotics 16:
9. Li H, Yi L, Leng C, Zhong Y, Hong J, Song X, Hao G (2024) Design of a Three-Axis Force Sensor

Using Decoupled Compliant Parallel Mechanisms. IEEE Sensors Journal
10. Yang M, Zhang C, Huang X, Chen S, Yang G (2021) A long-stroke nanopositioning stage with annular flexure guides. IEEE/ASME Transactions on Mechatronics 27:1570–1581
11. Zhu Z, To S, Zhu W-L, Li Y, Huang P (2018) Optimum Design of a Piezo-Actuated Triaxial Compliant Mechanism for Nanocutting. IEEE Trans Ind Electron 65:6362–6371
12. Wei H, Li W, Liu Y, Wang Y, Yang X (2017) Quasi-static analysis of a compliant tripod stage with plane compliant lever mechanism. Proceedings of the Institution of Mechanical Engineers, Part C: Journal of Mechanical Engineering Science 231:1639–1650
13. Wei H, Shirinzadeh B, Niu X, Zhang J, Li W, Simeone A (2021) Study of the hinge thickness deviation for a 316L parallelogram flexure mechanism fabricated via selective laser melting. Journal of Intelligent Manufacturing 32:1411–1420
14. Yang M, Zhang C, Yang G, Dong W (2019) Optimal design and tracking control of a superelastic flexure hinge based 3-PRR compliant parallel manipulator. IEEE Access 7:174236–174247
15. Zhu D, Zhan W (2019) Topology optimization of a 6-DOF spatial compliant mechanism based on Stewart propotype platform. Acta Mechanica Sinica 35:1044–1059
16. Chen G, Cheng Y, Bai R, Li B (2024) Two-Step Approach for Optimizing Flexure-Based Mechanisms: A Displacement Amplifier Case Study. IEEE/ASME Transactions on Mechatronics
17. Rommers J, van der Wijk V, Aragón AM, Herder JL (2024) The STAGE method for simultaneous design of the stress and geometry of flexure mechanisms. Precision Engineering 89:103–112
18. Zhu Z, Zhou X, Wang R, Liu Q (2015) A simple compliance modeling method for flexure hinges. Science China Technological Sciences 58:56–63
19. Yao J, Zu L, Ruan H, Cai D, Bai H, Xu Y, Zhao Y (2021) Stiffness modeling and force mapping analysis of hybrid-limb six-axis force sensor. Proceedings of the Institution of Mechanical Engineers, Part C: Journal of Mechanical Engineering Science 235:908–919
20. Qin Y-D, Shi Y-Y, Shirinzadeh B, Tian Y-L, Zhang D-W (2023) Characteristics of statically indeterminate symmetric flexure structures. Nanomanufacturing and Metrology 6:1
21. Panas RM, Sun F, Bekker L, Hopkins JB (2021) Combining cross-pivot flexures to generate improved kinematically equivalent flexure systems. Precision Engineering 72:237–249
22. Li R, Yang Z, Cai B, Chen G, Wu B, Wei Y (2022) A compliant guiding mechanism utilizing orthogonally oriented flexures with enhanced stiffness in degrees-of-constraint. Mechanism and Machine Theory 167:104555
23. Guo J, Lee K-M (2013) Compliant joint design and flexure finger dynamic analysis using an equivalent pin model. Mechanism and Machine Theory 70:338–353
24. Wei H, Shirinzadeh B, Li W, Clark L, Pinskier J, Wang Y (2017) Development of piezo-driven compliant bridge mechanisms: general analytical equations and optimization of displacement amplification. Micromachines 8:238
25. Qiu L, Yue X, Xie Z (2019) Design and analysis of Multicavity Flexure Hinge (MCFH) based on three-dimensional continuum topology optimization. Mechanism and Machine Theory 139:21–33
26. Wei H, Shirinzadeh B, Tang H, Niu X (2021) Closed-form compliance equations for elliptic-revolute notch type multiple-axis flexure hinges. Mechanism and Machine Theory 156:104154
27. Wei H, Yang J, Wu F, Niu X, Shirinzadeh B (2022) Analytical modelling and experiments for hybrid multiaxis flexure hinges. Precision Engineering 76:294–304
28. Ma F, Bai R, Chen G, Awtar S (2025) Nonlinear Complementary Strain Energy Formulation for Planar Beam Flexures Undergoing Intermediate Deflection. Journal of Mechanical Design 1–15
29. Ferrara-Bello A, Vargas-Chable P, Vera-Dimas G, Vargas-Bernal R, Tecpoyotl-Torres M (2021) XYZ micropositioning system based on compliance mechanisms fabricated by additive manufacturing. Actuators. https://doi.org/10.3390/act10040068
30. Dang MP, Le HG, Phan TTD, Chau NL, Dao TP (2022) Design and Optimization for a New XYZ Micropositioner with Embedded Displacement Sensor for Biomaterial Sample Probing Application. Sensors. https://doi.org/10.3390/s22218204
31. Shi H, Yang G, Li HN, Zhao J, Yu H, Zhang C (2024) A flexure-based and motion-decoupled XYZ nano-positioning stage with a quasi-symmetric structure. Precision Engineering 89:239–251
32. Li Y, Xu Q (2011) A totally decoupled piezo-driven XYZ flexure parallel micropositioning stage for micro/nanomanipulation. IEEE Transactions on Automation Science and Engineering 8:265–279
33. Zhu Z, To S, Zhu WL, Li Y, Huang P (2018) Optimum Design of a Piezo-Actuated Triaxial Compliant Mechanism for Nanocutting. IEEE Transactions on Industrial Electronics 65:6362–6371
34. Das TK, Shirinzadeh B, Ghafarian M, Al-Jodah A, Pinskier J (2020) Characterization of a compact piezoelectric actuated microgripper based on double-stair bridge-type mechanism. J Micro-Bio Robot 16:79–92
35. Wei H, Wang L, Niu X, Zhang J, Simeone A (2018) Fabrication, Experiments, and Analysis of an LBM Additive-Manufactured Flexure Parallel Mechanism. Micromachines 9:572
36. Ghafarian M, Shirinzadeh B, Al-Jodah A, Das TK, Wei W, Tian Y, Zhang D (2020) An XYZ micromanipulator for precise positioning applications. Journal of Micro-Bio Robotics 16:53–63
37. Calmé B, Rubbert L, Haddab Y (2022) Towards a compact XYZ θ positioning system with built-in actuators using 3D printing of conductive polymer. Journal of Micro-Bio Robotics 18:61–74
38. Lobontiu N, Garcia E (2003) Two-axis flexure hinges with axially-collocated and symmetric notches. Computers and Structures 81:1329–1341
39. Li L, Zhang D, Guo S, Qu H (2017) A generic compliance modeling method for two-axis

elliptical-arc-filleted flexure hinges. Sensors (Switzerland) 17:1–20
40. Wei H, Tian Y, Zhao Y, Ling M, Shirinzadeh B (2023) Two-axis flexure hinges with variable elliptical transverse cross-sections. Mechanism and Machine Theory 181:105183